Effect of gravity on nonlinear dynamics of the flow velocity field in turbulent fire

Kazushi Takagi and Hiroshi Gotoda*
Department of Mechanical Engineering, Tokyo University of Science, 6-3-1 Niijuku, Katsushika-ku, Tokyo 125-8585, Japan

(Received 8 July 2018; published 12 September 2018)

We numerically study the effect of gravity on the dynamic behavior of flow velocity field in a turbulent fire from the viewpoints of symbolic dynamics, statistical complexity, and complex networks. The randomness of streamwise flow velocity fluctuations significantly increases with increasing gravity, which is found to be correlated with the mean permutation entropy and the Froude number. The multiscale complexity-entropy causality plane clearly shows that under high gravity, high-dimensional deterministic chaos starts to be formed in the near field. We observe the appearance, disappearance, and reappearance of a scale-free structure in weighted networks between vortices under high gravity, clearly showing the presence of power-law decay in the lifetime of the scale-free structure.

DOI: 10.1103/PhysRevE.98.032207

I. INTRODUCTION

A wide variety of flame front instabilities emerge in a combusting flow as a result of the intimate interplay between the rapid chemical reaction, the convective motion of fluid, and the heat-mass diffusion, leading to the onset of intricate chaotic dynamics. In open diffusion flames, the overall flow field mainly consists of hot combustion products (low-density gas) outside flame front and cold surrounding quiescent air (high-density gas). Large density difference subjected to gravity can trigger a buoyant flow owing to a modified Kelvin-Helmholtz type hydrodynamic instability mechanism. This results in the formation of an upward toroidal vortex in the interface between two gases [1–3]. The strong interaction between the traveling toroidal vortex and flame front gives rise to significant deformation of flame front, leading to self-sustained flame front oscillations with large amplitude owing to the Rayleigh-Taylor instability mechanism [4]. These physical processes are known to have a significant impact on the generation and growth of a turbulent fire [5]. Thus far, a substantial number of numerical and experimental studies on buoyant plumes, buoyant jet diffusion flames, and pool fires have clarified the spatial distributions of the instantaneous and time-averaged flow velocity [6–12], vorticity [11,13,14], temperature [4,7,8,10–15], and turbulent statistics [7–9,12,16]. Most studies [4,6,14,15,17–22] have reported that the dominant oscillation frequency of flame front is strongly correlated with nondimensional numbers such as the Strouhal number, Froude number, and Richardson number.

Nonlinear time series analysis integrating chaos theory and fractal theory has become increasingly prevalent in the treatment of complex phenomena appearing in many areas of science and engineering, and has provided a crucial step towards an encompassing understanding and interpretation of the underlying dynamics. In fact, it has been proactively adopted for various flame front instabilities [23–27] and thermoacoustic combustion instabilities [28–37]. However, elucidation of the dynamic behavior of a buoyancy-driven turbulent fire using nonlinear time series analysis remains to be delineated. We have recently carried out a numerical study on the spatiotemporal behavior of a turbulent fire in terrestrial gravity and discovered two classes of nonlinear dynamics in flow velocity fluctuations: low-dimensional deterministic chaos in the near field dominated by the unstable motion of toroidal vortices and high-dimensional deterministic chaos in the far field forming a fully developed turbulent plume [38]. The existence of these dynamics was clearly verified using nonlinear time series analysis in terms of statistical complexity. Our primary interest in this work is to reveal the effect of gravity on the spatiotemporal evolution of a turbulent fire.

Our overarching objective here is to clarify how the gravity level alters the dynamical states of flow velocity fluctuations from the near field to the far field in a turbulent fire. To this end, we apply nonlinear time series analysis in terms of symbolic dynamics, complex networks, and statistical complexity. The permutation entropy [39] based on symbolic dynamics has become widely recognized by the nonlinear science community as a useful measure to quantify the randomness of irregular fluctuations. The applicability of the permutation entropy has been shown by Gotoda *et al.* [40]. In this study, we estimate the permutation entropy for temporal evolutions of flow velocity fluctuations under various gravity levels. In relation to the permutation entropy, another useful tool for analysis is the complexity-entropy causality plane (CECP) [41] based on statistical complexity. The CECP is represented by the permutation entropy and the Jensen-Shannon statistical complexity, and its extended version incorporating a time-dependent approach, namely the multiscale CECP [42], allows us to (i) quantify the degree of complexity at various time scales and (ii) test for the presence of chaotic dynamics in irregular fluctuations. The multiscale CECP has recently been introduced in combustion studies on flame front instability driven by buoyancy-swirl coupling [27] and thermoacoustic combustion oscillations [43]. In this study, we obtain the multiscale CECP to discuss the effect of gravity on the complexity of

*Corresponding author: gotoda@rs.tus.ac.jp

flow velocity fluctuations. The turbulence network [44], which maps vortex structures onto network structures consisting of nodes and edges, enables us to identify vortical interactions in a turbulent flow field from the viewpoint of complex networks. We adopt this turbulence network for the vorticity field in a turbulent fire to clarify how the scale-free structure related to fractality changes with increasing gravity. This paper has five parts. In Sec. II, a description of the governing equations is given with a summary of the numerical method used to solve the equations. In Sec. III, we describe the methodological framework of nonlinear time series analysis in terms of symbolic dynamics, statistical complexity, and complex networks. Our results and discussion are presented in Sec. IV. Finally, conclusions are given in Sec. V.

II. NUMERICAL SIMULATIONS

In accordance with previous studies [12,38], we conduct a large-eddy simulation of low-Mach-number flow to obtain the spatiotemporal dynamics of a buoyancy-driven turbulent fire. We numerically solve the following sets of governing equations: the mass conservation equation, the momentum conservation equation, the energy conservation equation, and the chemical species equations [45], considering the Smagorinsky model, a mixture fraction combustion model, and a global single-step irreversible chemical reaction involving CH_4, O_2, N_2, CO_2, and H_2O,

$$\frac{\partial \rho}{\partial t} + \nabla \cdot \rho \mathbf{u} = 0, \tag{1}$$

$$\rho\left(\frac{\partial \mathbf{u}}{\partial t} + (\mathbf{u}\cdot\nabla)\mathbf{u}\right) + \nabla p = \rho \mathbf{g} + \nabla \cdot \tau_v, \tag{2}$$

$$\frac{\partial}{\partial t}(\rho h) + \nabla \cdot \rho h \mathbf{u} = \frac{Dp}{Dt} + \dot{q}''' - \nabla \cdot \mathbf{q}_r + \nabla \cdot \lambda \nabla T + \sum_l \nabla \cdot h_l \rho D_l \nabla Y_l, \tag{3}$$

$$\frac{\partial}{\partial t}(\rho Y_l) + \nabla \cdot \rho Y_l \mathbf{u} = \nabla \cdot \rho D_l \nabla Y_l + \dot{m}_l''', \quad (l = 1, 2, \ldots, N_s). \tag{4}$$

Here, ρ is the density, t is the time, $\mathbf{u}$ $[=(u, v, w)]$ is the flow velocity vector, Y_l is the mass fraction of chemical species l, D_l is the diffusivity of chemical species l, $\dot{m}_l'''$ is the production rate of chemical species l per unit volume, p is the pressure, $\mathbf{g}$ is the gravitational acceleration vector, τ_v is the viscous stress tensor, h $(=T\sum_{l=1}^{N_s} c_{p,l} Y_l$, where $c_{p,l}$ is the specific heat capacity of chemical species l and N_s is the number of chemical species) is the enthalpy, $\dot{q}'''$ is the heat release rate per unit volume, which is approximated by a mixture fraction combustion model, $\mathbf{q}_r$ is the radiative heat flux vector, λ is the thermal conductivity, T is the temperature, and h_l is the enthalpy of chemical species l.

We adopt second-order finite differences for spatial derivatives and an explicit second-order predictor-corrector scheme for time derivatives in the governing equations. The finite volume method [46] is used to solve the radiative term in the energy conservation equation. Similarly to in our previous study [38], we set the computational domain in the x, y, and z directions to 2.0, 2.0, and 4.0 m, respectively. The total number of cells is 1 024 000 and a uniform grid of 2.5 cm is employed. Note that the sizes of the grid and the computational domain are the same as those in a numerical study conducted by Xin *et al.* [12]. The top and vertical boundaries of the computational domain are assumed to be open, allowing free inflow or outflow. The walls of the fire source with a hight of 0.05 m and the floor corresponding to the bottom plane outside the fire source both employ a nonslip and adiabatic boundary condition. The initial values of T, Y_{CH_4}, Y_{O_2}, and Y_{N_2} of the quiescent ambient air in the computational domain are set to 293 K, 0, 0.23, and 0.77, respectively. The mean axial flow velocity w_0 of gaseous fuel CH_4 from the fire source is estimated to 0.07 m/s. The time resolution in the computation is 1 ms. We perform nonlinear time series analysis on flow velocity fluctuations under various gravity levels. Although Xin *et al.* [12] computed the flow velocity field of 10 s, we analyze the flow velocity fluctuations for a sufficient interval of 28 s under a statistical stationary state after subtracting the initial transient obtained in the simulation. Note that in our preliminary test, we confirmed that the length of time series of flow velocity fluctuations does not affect the value of the permutation entropy when it exceeds 15 s for all the gravity levels considered in this study. The gravity level G $(=g_a/g)$ is varied from 1 to 10, where g_a is the gravitational acceleration in enhanced gravity and g is the gravitational acceleration in terrestrial gravity. The Froude number F_r, which is defined as the ratio of inertial and gravitational forces, is given by w_0^2/gGd [14,22], where d is the side length of the square fire source (=1 m).

III. MATHEMATICAL FRAMEWORK OF NONLINEAR TIME SERIES ANALYSIS BASED ON SYMBOLIC DYNAMICS, STATISTICAL COMPLEXITY, AND COMPLEX NETWORKS

A. Permutation entropy and complexity-entropy causality plane

The Shannon entropy is a well-recognized invariant describing the dynamical randomness in a nonlinear system. It is defined as the rate of production of information and is given by

$$S[\mathbf{P}] = \frac{-\sum_i p_i \log_2 p_i}{s_{\max}}, \quad \mathbf{P} = \{p_i; i = 1, 2, \ldots, M\}, \tag{5}$$

where p_i is a discrete probability function, M is the number of bins, and $S[\mathbf{P}]$ is the Shannon entropy normalized by $s_{\max}$. $s_{\max}$ $(=\log_2 M)$ corresponds to the Shannon entropy for completely random fluctuations with $\mathbf{P} = (1/M, 1/M, \ldots, 1/M)$. $S[\mathbf{P}]$ ranges from 0 to 1.

The permutation entropy [39] incorporating a symbolic dynamic approach takes into account the probability distribution of rank order patterns in the components of the phase space vectors as p_i. In this study, we estimate the permutation entropy $S_p[\mathbf{P}]$ for the D-dimensional phase space consisting of streamwise flow velocity fluctuations $\mathbf{w}(t) = (w'(t_i), w'(t_i + \tau), \ldots, w'[t_i + (D-1)\tau])$,

$$S_p[\mathbf{P}] = \frac{-\sum_{\pi_i} p(\pi_i) \log_2 p(\pi_i)}{s_{p,\max}}, \tag{6}$$

where $S_{p,\max}$ is the maximum permutation entropy ($= \log_2 D!$) and τ is the embedding delay time of the D-dimensional phase space. On the basis of a recent study [47], D is set to 5 in this study.

The CECP [41] based on the disequilibrium-based statistical complexity [48], which consists of the permutation entropy and the Jensen-Shannon statistical complexity, enables us to quantify the dynamical complexity. Zunino *et al.* [42] clearly showed that the multiscale CECP [42] incorporating a temporally scale-dependent approach is valid for investigating a presence of chaotic dynamics. In this study, we compute the multiscale CECP for the D-dimensional phase space consisting of $\mathbf{w}(t)$.

The Jensen-Shannon statistical complexity C_{JS} is defined as the product of S_p and the disequilibrium Q_J as follows:

$$C_{JS}[\mathbf{P}] = Q_J[\mathbf{P}, \mathbf{P}_e] S_p[\mathbf{P}] \tag{7}$$

$$Q_J[\mathbf{P}, \mathbf{P}_e] = \frac{S_p[(\mathbf{P}+\mathbf{P}_e)/2] - S_p[\mathbf{P}]/2 - S_p[\mathbf{P}_e]/2}{Q_{J,\max}} \tag{8}$$

$$Q_{JS,\max} = -\frac{1}{2}\left\{ \frac{D!+1}{D!} \log_2(D!+1) - 2\log_2(2D!) + \log_2 D! \right\}, \tag{9}$$

where $\mathbf{P_e}$ is a uniform probability distribution. If the dynamics represents deterministic chaos, the position of (S_p, C_{JS}) moves from the left-hand corner to the right-hand corner of the CECP as τ is increased, forming a parabolic curve on the CECP.

B. Turbulence network

A turbulence network [44] based on complex-network theory, in which weighted networks are constructed by connecting each fluid element to other fluid elements, is useful for clarifying vortical interactions in a turbulent flow field. In this work, we construct the turbulence network using the following adjacency matrix consisting of elements A_{ij}. Note that the turbulence network covers the entire region from the near field to the far field on the x-z plane (-0.7 m $\leqslant x \leqslant 0.7$ m, $y = 0$ m, and 0.3 m $\leqslant z \leqslant 3.6$ m),

$$A_{ij} = \begin{cases} \frac{U_{ij}+U_{ji}}{2}, & i \neq j, \\ 0, & i = j. \end{cases} \tag{10}$$

$$U_{ij} = \frac{|\Gamma_i|}{2\pi|\mathbf{x}_i - \mathbf{x}_j|} = \frac{|\omega(\mathbf{x}_i)\Delta x \Delta z|}{2\pi|\mathbf{x}_i - \mathbf{x}_j|}, \tag{11}$$

$$\omega = \frac{\partial w}{\partial x} - \frac{\partial u}{\partial z}. \tag{12}$$

Here, U_{ij} is the induced velocity from fluid element i on another element j, Γ_i is the circulation of fluid element i, $\omega(\mathbf{x}_i)$ is the vorticity, and $\mathbf{x}_i$ is the position vector of vertex i. We estimate the vertex strength distribution in the turbulence network as $s_i = \sum_j A_{ij}$. Δx and Δz are both 2.5 cm in this study.

IV. NUMERICAL RESULTS AND DISCUSSION

Figure 1 shows an instantaneous flow velocity field on the x-z plane in enhanced gravity $G = 3$ and temporal evolutions of the streamwise flow velocity w along the centerline of the fire source at different heights z in $G = 3$ and 10. When $G = 3$, aperiodic fluctuations of w are clearly observed at $z = 0.5$ m, corresponding to the continuous luminous zone [5]. The irregularity of w becomes large with increasing z. Irregular

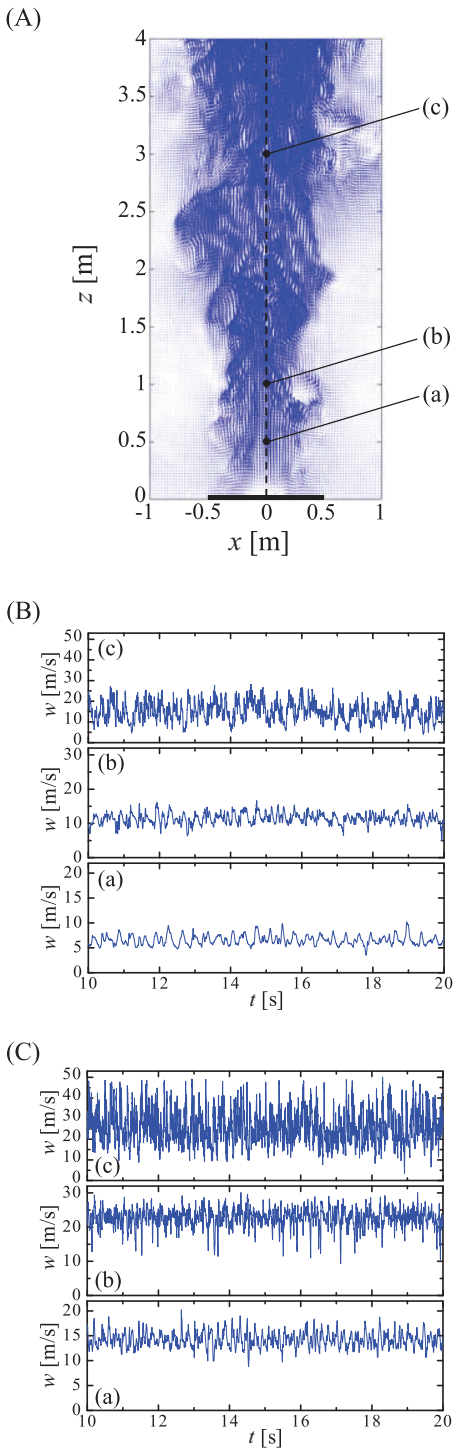

FIG. 1. Instantaneous flow velocity field on the x-z plane and temporal evolutions of streamwise flow velocity w along the centerline of the fire source at different heights z [(a) $z = 0.5$ m, (b) $z = 1.0$ m, and (c) $z = 3.0$ m] in enhanced gravity. (A) $G = 3$, (B) $G = 3$, and (C) $G = 10$.

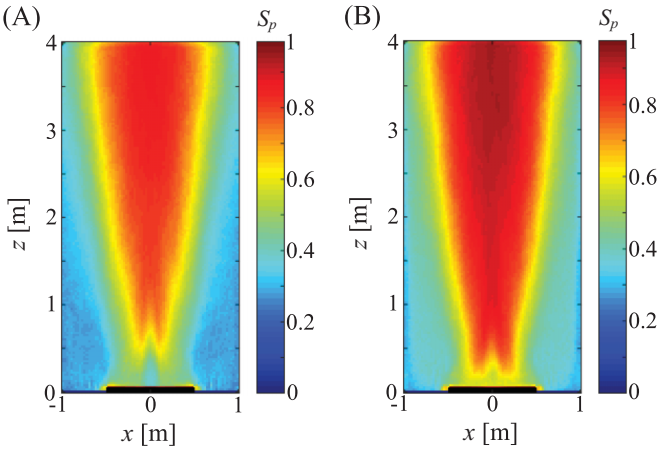

FIG. 2. Spatial distribution of the permutation entropy S_p for the temporal evolution of streamwise flow velocity fluctuations w' on the x-z plane in enhanced gravity. (A) $G = 3$ and (B) $G = 10$.

fluctuations of w at $z = 0.5$ m are attributed to unstable motion of transverse vortex rings owing to the buoyancy-driven Kelvin-Helmholtz instability of the interface between the combustion products and the surrounding quiescent air. These vortex rings in the near field are substantially deformed and broken down into smaller-scale eddies, leading to the breakdown of the continuous flame zone into an intermittent luminous zone [5]. This results in the appearance of larger irregularity in w at $z = 1.0$ m. Above this zone, a buoyancy-accelerated plume rapidly spreads owing to strong interactions of vortices with various scales. The formation of a fully developed turbulent plume causes the streamwise flow velocity to behave more irregularly in the far field ($z = 3.0$ m). When G is increased to 10, the mean value and the amplitude of w markedly increase at each z. According to a numerical simulation [14] on a laminar diffusion flame, the buoyant flow and the entrainment of oxygen mass flux into flame front are significantly strengthened under high gravity. This gives rise to increases in the local heat release of flame front and the density gradient, resulting in an increase in the amplitude of the streamwise flow velocity. We can adopt a similar argument to explain the significant increase in the amplitude of w during a turbulent fire under high gravity. The most interesting result here is the notable increase in the irregularity of w from the near field to the far field for $G = 10$, which means that gravity has a significant impact on the dynamics of a turbulent fire.

Figure 2 shows the spatial distribution of the permutation entropy S_p for the temporal evolution of streamwise flow velocity fluctuations w' on the x-z plane for $G = 3$ and 10. When $G = 3$, similar to the case of $G = 1$ [38], S_p for the far field is higher than that for the near field owing to the dynamics of smaller-scale vortices and isolated pockets, indicating a significant increase in the randomness of streamwise flow velocity fluctuations in the far field. When G is increased to 10, S_p markedly increases in the near field. This is accompanied by the rapid breakdown of unstable transverse vortex rings owing to the promotion of the buoyancy-driven Kelvin-Helmholtz instability and the Rayleigh-Taylor instability. Variation in the mean permutation entropy $\langle S_p \rangle$ in the near field and far field is shown in Fig. 3 as a function of the Froude number

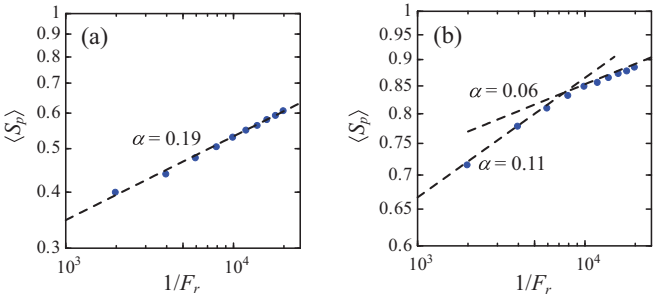

FIG. 3. Variation in the mean permutation entropy $\langle S_p \rangle$ as a function of the Froude number F_r for (a) the near field and (b) far field. (a) -0.5 m $\leqslant x \leqslant 0.5$ m, 0.3 m $\leqslant z \leqslant 0.5$ m, and (b) -0.5 m $\leqslant x \leqslant 0.5$ m, 3.0 m $\leqslant z \leqslant 3.6$ m.

F_r. Note that for the near field, -0.5 m $\leqslant x \leqslant 0.5$ m and 0.3 m $\leqslant z \leqslant 0.5$ m, while for the far field, -0.5 m $\leqslant x \leqslant 0.5$ m and 3.0 m $\leqslant z \leqslant 3.6$ m. As shown in Fig. 3(a), for the near field, $\langle S_p \rangle$ has a power-law relationship with $1/F_r$ whose scaling exponent α is about 0.19. As mentioned in Sec. I, a substantial number of studies on buoyant plumes and buoyant jet diffusion flames [4,6,14,15,17,19,21,22] have reported that the distinct oscillation frequency has a strong correlation with the Froude number, yielding $\mathrm{S}_t \propto F_r^{-a}$, where S_t is the Strouhal number and a is the scaling exponent. These studies [4,6,14,15,17,19,21,22] provided a useful scale model for characterizing the predominant mode produced by the buoyancy-driven Kelvin-Helmholtz instability. The empirical correlation we obtained from the viewpoint of symbolic dynamics, $\langle S_p \rangle \propto F_r^{-0.19}$ in the near field, is also useful for characterizing the complex dynamics of a buoyancy-driven turbulent fire. For the far field, $\langle S_p \rangle$ is significantly larger than the value for the near field at each $1/F_r$. The correlation exhibits different scaling laws from those for the near field with $\alpha = 0.11$ and 0.06. The effect of gravity on the randomness of streamwise flow velocity fluctuations in a fully developed turbulent plume regime changes at $1/F_r \sim 6\times10^3$. To the best of our knowledge, the empirical correlations consisting of the mean permutation entropy and the Froude number have not been proposed in previous combustion and fire studies.

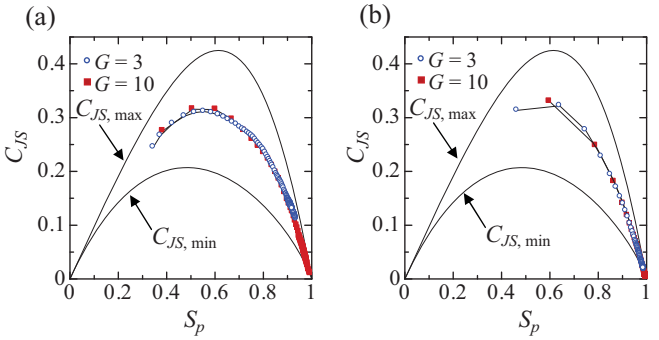

FIG. 4. Complexity-entropy causality planes of streamwise flow velocity fluctuations w' along the centerline of the fire source at different heights z [(a) $z = 0.5$ m and (b) $z = 3.0$ m] in enhanced gravity $G = 3$ and 10.

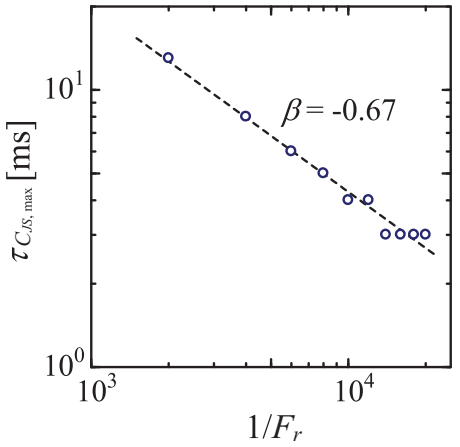

FIG. 5. Variation in the delay time $\tau_{C_{JS,\max}}$ as a function of the Froude number F_r for the near field ($z = 0.5$ m).

Figure 4 shows CECPs at $z = 0.5$ m and 3.0 m for $G = 3$ and 10, together with $C_{JS,\min}$ and $C_{JS,\max}$. When $G = 3$, for the near field ($z = 0.5$ m), a parabolic curve moving from left to right with increasing τ is clearly formed on the CECP. On the basis of a study by Zunino *et al.* [42], the dynamic behavior of w' in the near field represents low-dimensional deterministic chaos. When G is increased to 10, (S_p, C_{JS}) approaches the bottom right corner of the plane, showing a significant increase in complexity. For the far field ($z = 3.0$ m) with $G = 3$, the left-hand side of the curve becomes located in the middle to upper region of the plane and (S_p, C_{JS}) approaches the bottom right corner of the plane. This clearly shows the appearance of high-dimensional chaos. A similar trajectory is formed on the CECP when $G = 10$. We can conclude that high-dimensional chaotic dynamics more readily occurs with increasing gravity level. Zunino *et al.* [42] reported that the delay time $\tau_{C_{JS,\max}}$ at which C_{JS} takes a local maximum value corresponds to the minimum time scale required to capture complex dynamics. On this basis, we here investigate the relationship between $\tau_{C_{JS,\max}}$ extracted from the CECP and the gravity level. Variation in $\tau_{C_{JS,\max}}$ is shown in Fig. 5 as a function of F_r in the near field ($z = 0.5$ m). We observe interesting power-law decay with scaling exponent $\beta = -0.67$. This clearly shows that the complex dynamics of streamwise flow velocity fluctuations in the near field are correlated with the Froude number from the viewpoint of statistical complexity.

Figure 6 shows the instantaneous vorticity field and the spatial distribution of the vertex strength s when $G = 10$, together with the corresponding probability density function of the vertex strength $p(s)$. s significantly increases as the unstable transverse vortex rings are broken into smaller-scale vortices. This is due to an increase in connectivity between the vortices associated with the strong interactions of vortices with various scales. $p(s)$ exhibits power-law decay with spatial scaling exponent $\gamma = -4.3$, indicating the possible existence of a scale-free structure. In this study, we define that power-law decay of $p(s)$ appears when the coefficient of determinism for the scaling exponent $R^2 \geqslant 0.95$. An important point to note here is that the scale-free structure disappears and reappears over time during a turbulent fire. On the basis of this observation, we investigate the duration for which the scale-free structure is

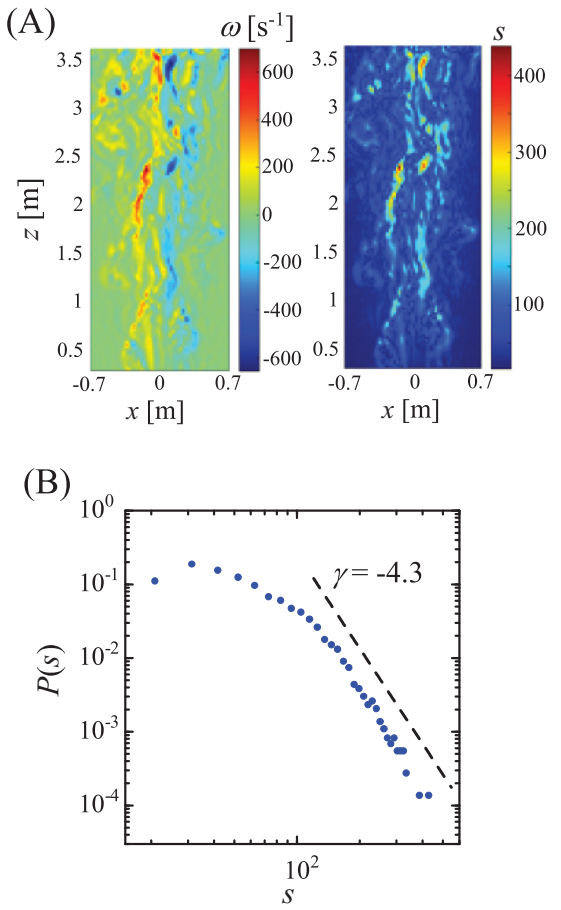

FIG. 6. (A) Instantaneous vorticity field and the corresponding spatial distribution of the vertex strength s in enhanced gravity $G = 10$. (B) Probability density function of the vertex strength in the turbulence networks $p(s)$ in enhanced gravity $G = 10$.

maintained under high gravity. Figure 7 shows the probability density function of the lifetime of the scale-free structure $p(\tau_d)$ when $G = 10$, where the lifetime τ_d is estimated as the remaining duration for which $R^2 \geqslant 0.95$ is satisfied for the scale-free structure. $p(\tau_d)$ clearly exhibits power-law decay with

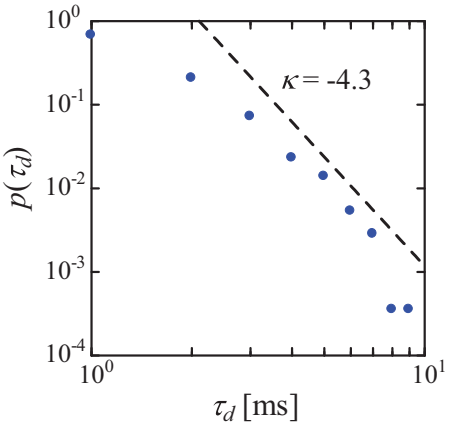

FIG. 7. Probability density function of the lifetime $p(\tau_d)$ of the scale-free structure in enhanced gravity $G = 10$.

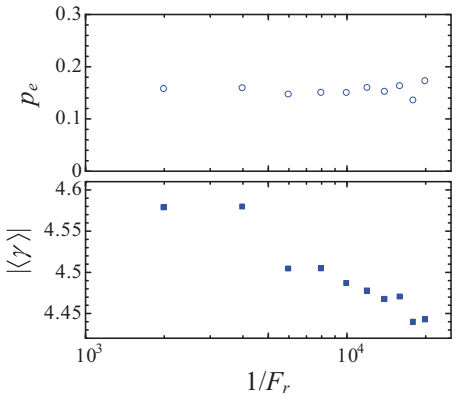

FIG. 8. Variations in the existence probability of scale-free structure P_e and absolute value of mean scaling exponent of vertex strength distribution $|\langle\gamma\rangle|$ as a function of the Froude number F_r.

temporal scaling exponent $\kappa = -4.3$. Variations in the existence probability of the scale-free structure P_e and the absolute value of the mean scaling exponent of the vertex strength distribution $|\langle\gamma\rangle|$ are shown in Fig. 8 as a function of F_r. P_e remains nearly unchanged with increasing F_r and its value is almost 0.16. This means that the enhanced gravity does not affect the extent of the onset of the scale-free structure, showing the appearance, disappearance, and reappearance of the scale-free structure. In contrast, $|\langle\gamma\rangle|$ significantly decreases when $1/F_r$ exceeds about 6×10^3. Interestingly, this critical value of $1/F_r$ corresponds to that classified by the empirical correlations: $\langle S_p\rangle \propto F_r^{\alpha}$ with scaling exponents $\alpha = 0.11$ and 0.06 (see Fig. 3). As mentioned above, the connectivity between the vortices increases as the interactions of vortices with various scales are strengthened, resulting in an increase in the vertex strength. The high vertex strength starts to appear when the gravity is substantially increased. The appearance of the high vertex strength reduces the existence probability of a lower vertex strength. As a result, $|\langle\gamma\rangle|$ significantly decreases with increasing $1/F_r$. In this paper, we have numerically studied the effect of gravity on the dynamic behavior of flow velocity field, showing the availability of nonlinear time series analysis as an alternative to the power spectrum analysis widely used in fire research. The findings obtained in this work are expected to help provide an encompassing understanding and interpretation of the complex dynamics in a buoyancy-driven turbulent fire.

V. CONCLUSIONS

We have studied the effect of gravity on the dynamic behavior of flow velocity field in a buoyancy-driven turbulent fire obtained by a three-dimensional large-eddy simulation from the viewpoints of symbolic dynamics, statistical complexity, and complex networks. The randomness of streamwise flow velocity fluctuations significantly increases with increasing gravity, which is found to be correlated with the mean permutation entropy and the Froude number. The multiscale complexity-entropy causality plane (CECP) incorporating a temporally scale-dependent approach clearly shows that under high gravity, high-dimensional chaotic dynamics starts to be formed in the near field dominated by the unstable motion of transverse vortex rings. The delay time at which the Jensen-Shannon statistical complexity takes a local maximum on the CECP for the near field exhibits power-law decay in terms of the inverse Froude number. The appearance, disappearance, and reappearance of a scale-free structure are observed in the turbulence network consisting of weighted networks between vortices, even under high gravity, clearly showing that the lifetime of the scale-free structure follows power-law decay.

ACKNOWLEDGMENT

This research was partially supported by the Private University Research Branding Project (2017-2021) from Ministry of Education, Culture, Sports, Science and Technology, Japan.

[1] L. D. Chen, J. P. Seaba, W. M. Roquemore, and L. P. Goss, Proc. Combust. Inst. **22**, 677 (1989).
[2] V. R. Katta and W. M. Roquemore, Combust. Flame **92**, 274 (1993).
[3] H. Gotoda, S. Kawaguchi, and Y. Saso, Exp. Therm. Fluid Sci. **32**, 1759 (2008).
[4] A. F. Ghoniem, I. Lakkis, and M. Soteriou, Proc. Combust. Inst. **26**, 1531 (1996).
[5] D. Drysdale, *An Introduction to Fire Dynamics* (Wiley, New York, 1994).
[6] B. M. Cetegen and K. D. Kasper, Phys. Fluids **8**, 2974 (1996).
[7] E. J. Weckman and A. B. Strong, Combust. Flame **105**, 245 (1996).
[8] S. R. Tieszen, T. J. O'Hern, R. W. Schefer, E. J. Weckman, and T. K. Blanchat, Combust. Flame **129**, 378 (2002).
[9] S. R. Tieszen, T. J. O'Hern, E. J. Weckman, and R. W. Schefer, Combust. Flame **139**, 126 (2004).
[10] P. E. DesJardin, T. J. O'Hern, and S. R. Tieszen, Phys. Fluids **16**, 1866 (2004).
[11] Y. Xin, J. P. Gore, K. B. McGrattan, R. G. Rehm, and H. R. Baum, Combust. Flame **141**, 329 (2005).
[12] Y. Xin, S. A. Filatyev, K. Biswas, J. P. Gore, R. G. Rehm, and H. R. Baum, Combust. Flame **153**, 499 (2008).
[13] R. W. Davis, E. F. Moore, W. M. Roquemore, L. D. Chen, V. Vilimpoc, and L. P. Goss, Combust. Flame **83**, 263 (1991).
[14] H. Sato, G. Kushida, K. Amagai, and M. Arai, Proc. Combust. Inst. **29**, 1671 (2002).
[15] W. E. Mell, K. B. McGrattan, and H. R. Baum, Proc. Combust. Inst. **26**, 1523 (1996).
[16] X. Zhou, K. H. Luo, and J. J. R. Williams, Combust. Flame **129**, 11 (2002).
[17] A. Hamins, J. C. Yang, and T. Kashiwagi, Proc. Combust. Inst. **24**, 1695 (1992).
[18] B. M. Cetegen and T. A. Ahmed, Combust. Flame **93**, 157 (1993).
[19] B. M. Cetegen, Y. Dong, and M. C. Soteriou, Phys. Fluids **10**, 1658 (1998).
[20] B. M. Cetegen and Y. Dong, Exp. Fluids **28**, 546 (2000).

[21] L. Hu, J. Hu, and J. L. de Ris, Combust. Flame **162**, 1095 (2015).
[22] H. Abe, A. Ito, and H. Torikai, Proc. Combust. Inst. **35**, 2581 (2015).
[23] H. Gotoda, T. Miyano, and I. G. Shepherd, Phys. Rev. E **81**, 026211 (2010).
[24] H. Gotoda, T. Ikawa, K. Maki, and T. Miyano, Chaos **22**, 033106 (2012).
[25] L. K. B. Li and M. P. Juniper, Proc. Combust. Inst. **34**, 947 (2013).
[26] H. Kinugawa, K. Ueda, and H. Gotoda, Chaos **26**, 033104 (2016).
[27] H. Gotoda, H. Kobayashi, and K. Hayashi, Phys. Rev. E **95**, 022201 (2017).
[28] L. Kabiraj, A. Saurabh, P. Wahi, and R. I. Sujith, Chaos **22**, 023129 (2012).
[29] V. Nair and R. I. Sujith, Chaos **23**, 033136 (2013).
[30] V. Nair, G. Thampi, and R. I. Sujith, J. Fluid Mech. **756**, 470 (2014).
[31] K. Kashinath, I. C. Waugh, and M. P. Juniper, J. Fluid Mech. **761**, 399 (2014).
[32] H. Gotoda, Y. Okuno, K. Hayashi, and S. Tachibana, Phys. Rev. E **92**, 052906 (2015).
[33] L. Kabiraj, A. Saurabh, N. Karimi, A. Sailor, E. Mastorakos, A. P. Dowling, and C. O. Paschereit, Chaos **25**, 023101 (2015).
[34] S. Balusamy, L. K. B. Li, Z. Han, M. P. Juniper, and S. Hochgreb, Proc. Combust. Inst. **35**, 3229 (2015).
[35] J. Tony, E. A. Gopalakrishnan, E. Sreelekha, and R. I. Sujith, Phys. Rev. E **92**, 062902 (2015).
[36] S. Suresha, R. I. Sujith, B. Emerson, and T. Lieuwen, Phys. Rev. E **94**, 042206 (2016).
[37] R. Sampath, M. Mathur, and S. R. Chakravarthy, Phys. Rev. E **94**, 062209 (2016).
[38] K. Takagi, H. Gotoda, I. T. Tokuda, and T. Miyano, Phys. Rev. E **96**, 052223 (2017).
[39] C. Bandt and B. Pompe, Phys. Rev. Lett. **88**, 174102 (2002).
[40] H. Gotoda, M. Pradas, and S. Kalliadasis, Phys. Rev. Fluids **2**, 124401 (2017).
[41] O. A. Rosso, H. A. Larrondo, M. T. Martin, A. Plastino, and M. A. Fuentes, Phys. Rev. Lett. **99**, 154102 (2007).
[42] L. Zunino, M. C. Soriano, and O. A. Rosso, Phys. Rev. E **86**, 046210 (2012).
[43] S. Murayama, H. Kinugawa, I. T. Tokuda, and H. Gotoda, Phys. Rev. E **97**, 022223 (2018)
[44] K. Taira, A. G. Nair, and S. L. Brunton, J. Fluid Mech. **795**, R2 (2016).
[45] K. B. McGrattan, H. R. Baum, R. G. Rehm, A. Hamins, and G. P. Forney, Fire dynamics simulator-Technical reference guide, National Institute of Standards and Technology, Report No. NISTIR6467, 2000; K. B. McGrattan, Fire dynamics simulator (version 4)-Technical reference guide, National Institute of Standards and Technology, NIST Special Publication Report No. 1018, 2006.
[46] S. H. Kim and K. Y. Huh, Numer. Heat Transfer, Part B **35**, 85 (1999).
[47] C. W. Kulp and L. Zunino, Chaos **24**, 033116 (2014).
[48] P. W. Lamberti, M. T. Martin, A. Plastino, and O. A. Rosso, Physica A **334**, 119 (2004).